High-Order bound-preserving discontinuous Galerkin methods for wormhole propagation on triangular meshes*

Ziyao Xu†, Yang Yang‡, Hui Guo§

Abstract

Wormhole propagation, arising in petroleum engineering, is used to describe the distribution of acid and the increase of porosity in carbonate reservoir under dissolution of injected acid. The important physical features of porosity and acid concentration include their boundedness between 0 and 1, as well as the monotone increasing for porosity. How to keep these properties in the simulation is crucial to the robustness of the numerical algorithm. In this paper, we propose high-order bound-preserving discontinuous Galerkin methods to keep these important physical properties. The main technique is to introduce a new variable r to replace the original acid concentration and use a consistent flux pair to deduce a ghost equation such that the positive-preserving technique can be applied on both original and deduced equations. A high-order slope limiter is used to keep a polynomial upper bound which changes over time for r. Moreover, the high-order accuracy is attained by the flux limiter. Numerical examples are given to demonstrate the high-order accuracy and bound-preserving property of the numerical technique.
Key Words: wormhole propagation, bound-preserving, high-order, discontinuous Galerkin method, triangular meshes, flux limiter

1 Introduction

As an important technique of enhanced oil recovery (EOR), acid treatment has been widely practiced in carbonate reservoir to improve the productivity of oil wells. In this technique, acid is injected into wells to dissolve the fines deposed in wellbore and the rock near the wellbore. By doing so, the permeability and porosity of the rock close to a well can be increased prominently, which facilitates oil flow into production well and thereby improves the production rate of oil.

†Department of Mathematical Sciences, Michigan Technological University, Houghton, MI 49931. E-mail: ziyaox@mtu.edu
‡Department of Mathematical Sciences, Michigan Technological University, Houghton, MI 49931. E-mail: yyang7@mtu.edu
§College of Science, China University of Petroleum, Qingdao 266580, China. E-mail: sdugh@163.com

However, the efficiency of this technique has a strong relevance with the dissolution patterns which depend on the injection rate. With a very low injection rate, the acid only dissolves the face of wellbore since it will be consummated all before they get into deeper region and this scenario is called face dissolution pattern. In contrast, with a very high injection rate, the acid can be pushed uniformly into the wellbore region with certain depth and this results is the so-called uniform dissolution pattern. In addition to the above two extreme cases, with an appropriate injection rate, wormhole patterns can be formed as the injected acid in the rock tends to flow through the paths with high permeability and porosity, which causes the permeability and porosity of these path to be further increased under the dissolution of acid, and facilitate more acid to flow through. Therefore, under optimal injection rate, maximum number of narrow channels with high conductivity will be formed in the rocks after the acidizing process. These highly conducting channels, also known as wormholes because of its shape, can build a good connectivity between reservoir and wellbore, and improve the productivity of oil well enormously. Because of the important role that wormhole plays in improving productivity, a lot of research works have been taken to investigate the formation and propagation of wormholes.

In the early days, researchers investigated the wormhole propagation phenomenon by means of experiments [11, 5]. Later, several mathematical models, such as dimensionless model, capillary tube model, network model, and continuum models, were established to help people understand the process of wormhole propagation. Among these models, the most popular one is the two-scale continuum model developed by Panga et al. in [16], where the authors proposed a partial differential equations (PDE) system to describe the formation and propagation of wormholes. There were a lot of follow-up works based on this model. In [33], the authors analyzed the front instability of wormhole propagation theoretically and numerically. In [15], Maheshwari et al. presented a 3D simulation for this model. A parallel simulation was conducted by Wu et al. in [21] under a modification of flow equation. In [1], the authors studied the numerical-simulation approach for a modified model. Later, Wei et al. extended this model from single phase to two-phase flow in [19] and discussed the simulation results. Besides the above, many researchers designed specific numerical schemes for this kind of models as well. In [12], the authors constructed a conservative scheme for flow and transport based on mixed finite element method. Later, Li et al. applied finite difference methods to this problem in [13, 14]. Recently, the discontinuous Galerkin (DG) method was applied to this model in [8]. In all the above works, some theoretical works, such as the stability and error estimates, were established under different norms. However, to the best of our knowledge, no works has been undertaken to preserve the boundedness of porosity and concentration of acid without loss of mass conservative. In fact, the boundedness of these variables is essential for the stability of numerical simulations. Firstly, the rate of change of porosity ϕ in this model depends on the concentration of acid c_f. If the exact solutions contain large gradients or even discontinuities, the numerical approximations of c_f can be negative, which further leads to $\phi < 0$ in some regions with low porosity. Secondly, the oscillations of ϕ itself near the wormhole may also result in negative values. Both of the above two cases will bring a negative coefficient in the diffusion term of the transport equation, leading to ill-posedness of the problems, and finally cause the blow-up of the numerical simulations. We will demonstrate this feasibility by a numerical example in Section 6 and show how bound-preserving technique can prevent the blow-up phenomenon. Moreover, as we will see in the later section, many coefficients in the model appear as functions of ϕ, which require ϕ to take values in the physically relevant range $[0, 1]$ as well. To construct high-order bound-preserving technique, we have to apply suitable limiters to modify the numerical approximations. Therefore, we would like to use DG methods.

The DG methods become increasingly popular due to their good stability, high-order accuracy, and flex-

ibility on h-p adaptivity. In 2010, the genuinely maximum-princip le-satisfying high-order DG schemes were constructed for conservation laws on rectangular meshes in [29] by Zhang and Shu. The basic idea is to take the test function to be 1 in each cell to yield an equation satisfied by the cell average of the target variable r, and prove the desired boundedness of the cell average $\bar{r}$. Then a slope limiter which do not affect accuracy and mass conservation can be used to modify the variable r to obtain a new one $\tilde{r} = \bar{r} + \theta(r - \bar{r})$ such that $\tilde{r}$ has the physically relevant bounds. In the case that the variable r only need a lower bound zero, this technique is also called positivity-preserving technique. The physically positivity-preserving and bound-preserving numerical schemes have been actively studied since then. In 2012, this technique has been successfully extended to triangular meshes in [30], where the general criteria for quadrature rule on triangular elements was proposed. After that, this technique was applied to many problems including compressible Euler equations with source terms [31], hyperbolic equations involving δ-singularities [26, 27], relativistic hydrodynamics [17], extended MHD equations [34], shallow water equations [22], etc. For convection-diffusion equations, the genuinely second-order maximum-principle-preserving technique were introduced in [32]. Subsequently, the extension to third-order or even higher order bound-preserving techniques for parabolic equations were also developed in [25, 2, 4]. Besides the above, the flux limiter [24, 23, 10] can also be used to obtain the high-order accuracy and maintain the boundedness. However, with the flux limiters we have to modify the numerical fluxes, hence the accuracy is not easy to analyze. Recently, in [9, 3], the authors studied miscible displacements in porous media and applied the techniques introduced in [32, 10, 23, 24] to preserve the two bounds, 0 and 1, of the volumetric fractions. In this paper, we will construct high-order bound-preserving DG schemes for the porosity of the rocks ϕ and the concentration of the acid c_f. However, there are significant differences from most of the previous techniques. First of all, most of the problems in [24, 29] satisfy maximum-principles while the concentration of acid c_f does not. To solve this problem, we derive a ghost equation satisfied by $c = 1 - c_f$ and apply the positivity-preserving technique to both c_f and c. Secondly, the high-order positivity-preserving technique in this paper is based on the flux limiter [23, 10]. The basic idea is to combine higher order and lower order fluxes to construct a new one which can yield positive numerical cell averages. However, for triangular meshes, first-order fluxes are not easy to construct. Therefore, we will consider the second-order flux as the lower order one. Moreover, to obtain the equation satisfied by the cell averages, we need to numerically approximate $r = \phi c_f$ instead of c_f. By doing so, the upper bound of r is not a constant and the traditional slope limiter may fail to work [9]. Therefore, a new bound-preserving limiter will be introduced. A similar obstacle appeared in the design of high-order bound-preserving methods for general relativistic hydrodynamics, see [20] for the discussion. Finally, different from [9, 3], the porosity is increasing and less than 1. Therefore, the upper bound of r is changing during time evolution and special techniques will be introduced to make ϕ to be physically relevant. In summary, the whole algorithm can be separated into four parts. We first apply positivity-preserving technique to obtain positive ϕ_t and use which as another source to find the velocity and pressure. Then apply the positivity-preserving technique again to ϕ and c_f simultaneously to obtain positive numerical cell averages by the flux limiter [23, 10]. Subsequently, we choose consistent flux pair [9, 3] with suitable parameters in the flux limiter in the concentration and pressure equations to obtain the positivity of $1 - c_f$. Finally, we introduce suitable limiters to obtain physically relevant numerical approximations.

The rest of the paper is organized as follows. In Section 2, we introduce the mathematical model of wormhole propagation. In Section 3, we establish the DG scheme used in this paper. In Sections 4 and 5, we construct the second-order bound-preserving scheme and then extend it to high-order spatial and time discretizations. Some numerical examples are given in Section 6. We will end in Section 7 with some

3

concluding remarks.

2   Mathematical model

Let the computational domain $\Omega = [0, 2\pi] \times [0, 2\pi]$ and simulation time $J = [0, T]$, the mathematical model of the wormhole propagation is given as follows:

$$\frac{\partial \phi}{\partial t} + \nabla \cdot \mathbf{u} = f, \quad (x, y) \in \Omega, \ 0 < t \le T, \tag{2.1}$$

$$\mathbf{u} = \frac{-\kappa(\phi)}{\mu} \nabla p, \quad (x, y) \in \Omega, \ 0 < t \le T, \tag{2.2}$$

$$\frac{\partial (\phi c_f)}{\partial t} + \nabla \cdot (\mathbf{u} c_f) = \nabla \cdot (\phi \mathbf{D} \nabla c_f) + k_c a_v (c_s - c_f) + f_I c_I - f_P c_f, \tag{2.3}$$

$$\frac{\partial \phi}{\partial t} = \frac{\alpha k_c a_v (c_f - c_s)}{\rho_s}, \quad (x, y) \in \Omega, \ 0 < t \le T, \tag{2.4}$$

where ϕ is the porosity which is defined as the percentage of the empty space in a rock, κ is the permeability that measures the ability for a rock to allow fluid to pass through it, $\boldsymbol{u}$ is the Darcy's velocity defined as the volume of flow crossing a unit across-section per unit time, p is the pressure of fluid in porous media, and μ is the viscosity of fluid. $f = f_I - f_P$ is the external volumetric flow rate with $f_I = \max\{f, 0\}$ being the injection flow rate and $f_P = -\min\{f, 0\}$ being the production flow rate. c_f, c_s and c_I are the concentrations of acid in the fluid phase, the fluid-solid interface and in the injected flow, respectively. $\mathbf{D}$ is the dispersion tensor for the acid in porous media and k_c is the local mass-transfer coefficient. a_v is the interfacial area available for reaction, ρ_s is the density of the rock and α is the dissolving constant of the acid, defined as grams of solid dissolved per mole of acid reacted. Moreover, in the case of first order kinetic reaction, the concentration c_s of acid in the fluid-solid interface have a simple relationship with c_f:

$$c_s = \frac{c_f}{1 + k_s/k_c},$$

where k_s is the kinetic constant for reaction. The coefficients κ and a_v are functions of ϕ defined as

$$\frac{\kappa}{\kappa_0} = \frac{\phi}{\phi_0} \left(\frac{\phi(1 - \phi_0)}{\phi_0(1 - \phi)} \right)^2, \quad \frac{a_v}{a_0} = \frac{1 - \phi}{1 - \phi_0}, \tag{2.5}$$

respectively, where κ_0, a_0, and ϕ_0 are the initial values for κ, a_v, ϕ. Throughout this paper, the values $\mu, k_c, k_s, \alpha, \rho_s$ are positive constants, $\mathbf{D}, f, f_I, f_P, c_I$ are known functions independent of time and $\phi, \boldsymbol{u}, p, c_f$, are unknown time-dependent variables.

We consider impermeable boundary conditions

$$\mathbf{u} \cdot \mathbf{n} = 0, \quad (\mathbf{D} \nabla c - c \mathbf{u}) \cdot \mathbf{n} = 0,$$

where $\mathbf{n}$ is the unit outer normal of the boundary $\partial \Omega$. The initial concentration and porosity are given as

$$c_f(x, y, 0) = c_0(x, y), \quad \phi(x, y, 0) = \phi_0(x, y), \quad (x, y) \in \Omega.$$

Before we finish this section ,we would like to make an important reasonable hypothesis for the initial porosity: $0 < \phi_\star \le \phi_0(x, y) \le \phi^\star < 1$.

3 The DG scheme

In this section, we will construct the DG scheme for wormhole propagation on triangular meshes. We first demonstrate the notations to be used throughout the paper.

Consider a regular triangulation Ω_h of domain Ω, i.e. $\exists \rho > 0$, such that $\text{diam}(B_K) \geq \rho\,\text{diam}(K), \forall K \in \Omega_h$, where B_K is the largest ball contained in K. For any triangle $K \in \Omega_h$, we denote the three edges of K to be e_K^i ($i = 1, 2, 3$), with corresponding lengths ℓ_K^i ($i = 1, 2, 3$), unit outer normal vectors $\boldsymbol{\nu}_K^i$ ($i = 1, 2, 3$) and neighboring elements $K_i (i = 1, 2, 3)$. We denote $\Gamma = \bigcup_{K \in \Omega_h} \{e | e \in \partial K\}$ to be the set of all cell interfaces and $\Gamma_0 = \Gamma \setminus \partial \Omega_h$ as all the interior ones. Set a predetermined constant unit vector $\boldsymbol{\nu}_0$ which is not parallel to any edge e and define $\boldsymbol{n}_e$ as the unit normal vector of each edge $e \in \Gamma$ such that $\boldsymbol{n}_e \cdot \boldsymbol{\nu}_0 > 0$. For any discontinuous function v (scalar or vector) crossing edge e, let $v_e^{\pm}$ denote its traces on e evaluated from K or K_i . The $'\pm'$ for each edge e_K^i in the cell K is determined by the inner product of $\boldsymbol{\nu}_K^i$ and $\boldsymbol{\nu}_0$ as follows:

$$v_e^- = v_K, \quad v_e^+ = v_{K_i}, \quad \text{if } \boldsymbol{\nu}_0 \cdot \boldsymbol{\nu}_K^i > 0,$$

$$v_e^+ = v_K, \quad v_e^- = v_{K_i}, \quad \text{if } \boldsymbol{\nu}_0 \cdot \boldsymbol{\nu}_K^i < 0.$$

Moreover, we define the jump and average of v (either a scalar or a vector) on the cell interface e as

$$[v]_e = v_e^+ - v_e^-, \quad \{v\}_e = \frac{1}{2}(v_e^+ + v_e^-).$$

The finite element spaces are chosen as

$$V_h = \{v : v|_K \in P^k(K), \ \forall K \in \Omega_h\} \text{ and } W_h = V_h \times V_h,$$

where $P^k(K)$ denotes the space of polynomials of degree at most k in K. Then the semidiscrete DG scheme for (2.1) - (2.4) can be written as: find $\phi, r, p \in V_h$ and $\boldsymbol{u} \in W_h$ such that for any $\zeta, \xi, v \in V_h$ and $\boldsymbol{\eta} \in W_h$, the following equations hold:

$$\left(\frac{\partial \phi}{\partial t}, \zeta\right) = (\mathbf{u}, \nabla \zeta) + \sum_{e \in \Gamma_0} \int_e \hat{\mathbf{u}} \cdot \boldsymbol{n}_e [\zeta] ds + (f, \zeta), \tag{3.1}$$

$$(a(\phi)\mathbf{u}, \boldsymbol{\eta}) = (p, \nabla \cdot \boldsymbol{\eta}) + \sum_{e \in \Gamma} \int_e \hat{p}\,\boldsymbol{n}_e \cdot [\boldsymbol{\eta}] ds, \tag{3.2}$$

$$\left(\frac{\partial r}{\partial t}, \xi\right) = (\mathbf{u}c_f - \phi D \nabla c_f, \nabla \xi) + \sum_{e \in \Gamma_0} \int_e \widehat{\mathbf{u}c_f} \cdot \boldsymbol{n}_e [\xi] ds + (f_I c_I - f_P c_f - B_1(\phi)c_f, \xi)$$

$$- \sum_{e \in \Gamma_0} \int_e \left(\{\phi \boldsymbol{D}(\boldsymbol{u})\nabla c_f\} \cdot \boldsymbol{n}_e [\xi] + \{\phi \boldsymbol{D}(\boldsymbol{u})\nabla \xi\} \cdot \boldsymbol{n}_e [c_f] + \frac{\tilde{\alpha}}{|e|}[c_f][\xi]\right) ds, \tag{3.3}$$

$$\left(\frac{\partial \phi}{\partial t}, v\right) = (B_2(\phi)c_f, v), \tag{3.4}$$

where

$$a(\phi) = \frac{\mu}{k}, B_1(\phi) = \frac{a_0(1-\phi)k_s k_c}{(1-\phi_0)(k_s+k_c)}, B_2(\phi) = \frac{\alpha a_0(1-\phi)k_s k_c}{\rho_s(1-\phi_0)(k_s+k_c)}.$$

Moreover, we use a new variable r instead of ϕc_f on the left hand side of (3.3), and define c_f as the L^2-projection of $\frac{r}{\phi}$ if $k \geq 2$, while take c_f to be the interpolation of $\frac{r}{\phi}$ at the three vertices in each triangle K if $k = 1$.

Following the idea in [9, 3], we take a consistent flux pair $\hat{\boldsymbol{u}}, \widehat{\boldsymbol{u}c_f}$ in the sense that $\hat{\boldsymbol{u}} = \widehat{\boldsymbol{u}c_f}$ when $c_f = 1$. The consistent flux pair is used in the construction of the bound-preserving techniques. The numerical fluxes $\hat{\boldsymbol{u}}, \widehat{\boldsymbol{u}c_f}$ and $\hat{p}$ in (3.1)-(3.4) are chosen as

$$\hat{\mathbf{u}}|_e = \{\mathbf{u}\}_e, \quad \hat{p}|_e = \{p\}_e, \quad \widehat{\mathbf{u}c_f}|_e = \{\mathbf{u}c_f\}_e - \alpha[c_f]_e\mathbf{n}_e, \quad \text{if } e \in \Gamma_0,$$

$$\hat{\mathbf{u}}|_e = 0, \quad \hat{p}|_e = p_K, \quad \widehat{\mathbf{u}c_f}|_e = 0, \quad \text{if } e \in \partial\Omega \cap \partial K. \tag{3.5}$$

In the DG schemes, we introduced two penalty parameters α and $\tilde{\alpha}$. These two parameters will be chosen by the bound-preserving technique.

4   Second-order bound-preserving schemes

In this section, we will construct second-order bound-preserving scheme with forward Euler time discretization. High-order time discretizations will be discussed in the next section. At time level n, we assume $\phi^0 < \phi^n < 1$ and $0 \le r^n \le \phi^n$, and would like to construct physically relevant numerical approximations at time level $n + 1$, i.e. $\phi^n \le \phi^{n+1} < 1$ and $0 \le r^{n+1} \le \phi^{n+1}$.

At time level n, we will first solve (3.4) for ϕ_t^n, then substitute which to the left-hand side of (3.1). With forward Euler time discretization, (3.1), (3.3) and (3.4) can be written as

$$\left(\frac{\phi^{n+1} - \phi^n}{\Delta t}, \zeta\right) = (\mathbf{u}, \nabla\zeta) + \sum_{e \in \Gamma_0} \int_e \hat{\mathbf{u}} \cdot \boldsymbol{n}_e[\zeta]ds + (f, \zeta), \tag{4.1}$$

$$\left(\frac{r^{n+1} - r^n}{\Delta t}, \xi\right) = (\mathbf{u}c_f - \phi\mathbf{D}\nabla c_f, \nabla\xi) + \sum_{e \in \Gamma_0} \int_e \widehat{\mathbf{u}c_f} \cdot \boldsymbol{n}_e[\xi]ds + (f_I c_I - f_P c_f - B_1(\phi)c_f, \xi)$$

$$- \sum_{e \in \Gamma_0} \int_e \left(\{\phi\boldsymbol{D}(\mathbf{u})\nabla c_f\} \cdot \boldsymbol{n}_e[\xi] + \{\phi\boldsymbol{D}(\mathbf{u})\nabla\xi\} \cdot \boldsymbol{n}_e[c_f] + \frac{\tilde{\alpha}}{|e|}[c_f][\xi]\right) ds, \tag{4.2}$$

$$\left(\frac{\phi^{n+1} - \phi^n}{\Delta t}, v\right) = (B_2(\phi)c_f, v), \tag{4.3}$$

with all the superscript n on the right hand sides being omitted for simplicity.

Remark 4.1. *After the time discretization, there are two discrete evolution equations for ϕ. We use (4.3) to find ϕ^{n+1}, then the discrete evolution for ϕ in (4.1) is treated as another source.*

Because of the usage of consistent flux pair $\hat{\boldsymbol{u}}$ and $\widehat{\boldsymbol{u}c_f}$, we can get a ghost equation for r_2 by subtracting (4.2) from (4.1) and introducing ghost variables $c_2 = 1 - c_f, c_{2I} = 1 - c_I, r_2 = \phi c_2$,

$$\left(\frac{r_2^{n+1} - r_2^n}{\Delta t}, \xi\right) = (\mathbf{u}c_2 - \phi\mathbf{D}\nabla c_2, \nabla\xi) + \sum_{e \in \Gamma_0} \int_e \widehat{\mathbf{u}c_2} \cdot \boldsymbol{n}_e[\xi]ds + (f_I c_{2I} - f_P c_2 + B_1(\phi)c_f, \xi)$$

$$- \sum_{e \in \Gamma_0} \int_e \left(\{\phi\boldsymbol{D}(\mathbf{u})\nabla c_2\} \cdot \boldsymbol{n}_e[\xi] + \{\phi\boldsymbol{D}(\mathbf{u})\nabla\xi\} \cdot \boldsymbol{n}_e[c_2] + \frac{\tilde{\alpha}}{|e|}[c_2][\xi]\right) ds. \tag{4.4}$$

Therefore, though we solve (4.1) and (4.2) in the real computation, we analyze (4.2) and (4.4) instead of the former pair as the two forms are equivalent.

The second-order bound-preserving scheme is built and analyzed based on (4.2), (4.4) and (4.3).

In this paper, we use the quadrature rule of order k proposed in [28] to compute the integral in cells, and
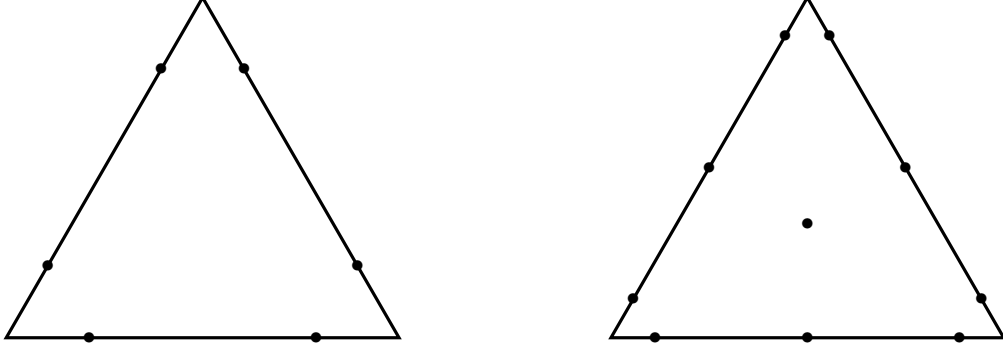
Figure 1: Distribution of quadrature points for $k = 1$ and $k = 2$.

use the corresponding $k + 1$ points Gaussian quadrature rule to evaluate integration on cell interfaces. The quadrature rule of order k has the following crucial properties:

- All of the quadrature points lie in the cells with positive weights,

- The quadrature points contains $k + 1$ Gaussian quadrature points in each of its edges,

- It is exact for polynomials up to degree $2k - 1$,

The distribution of quadrature points in the case of $k = 1$ and $k = 2$ are shown in Figure 1. We denote $x_{i,\beta}$, $\beta = 1, 2, \cdots, k + 1$, as the quadrature points on e_K^i with $\tilde{w}_\beta$ being the corresponding weights, and denote x_γ, $\gamma = 1, 2, \cdots, L$, as the quadrature points in cell K with $\hat{\omega}_\gamma$ being the corresponding weights. Moreover, We denote ω_β, $\beta = 1, 2, \cdots, k + 1$, as the $k + 1$ Gaussian quadrature weights on the reference interval $[-\frac{1}{2}, \frac{1}{2}]$. Based on the above notations, we define the values of o ($o = r, c, \phi, p, \cdots$) at the quadrature points as $o_K^{i,\beta} = o(x_{i,\beta})$ along the boundary of K and $o_K^\gamma = o(x_\gamma)$ in cell K.

In (3.4), we take $v = 1$ in K to obtain the equation satisfied by the cell average of ϕ:

$$\bar{\phi}_K^{n+1} = \bar{\phi}_K^n + \triangle t \overline{B_2(\phi^n) c_f}. \tag{4.5}$$

We will demonstrate how to preserve the monotonicity and the upper bound of $\bar{\phi}_K^{n+1}$ in the following lemma:

Lemma 4.1. *Given* $0 \leq r^n \leq \phi^n$ ($0 \leq c_f^n \leq 1$) *and* $\phi^n < 1$, *we have* $\bar{\phi}_K^n \leq \bar{\phi}_K^{n+1} < 1$, *if the time step satisfies*

$$\triangle t < B_{30}^{-1}, \tag{4.6}$$

where B_{30} *is a constant defined as*

$$B_{30} = \frac{\alpha a_0 k_s k_c}{\rho_s (1 - \phi^\star)(k_s + k_c)}.$$

Proof. Define $B_3(x) = \frac{\alpha a_0 k_s k_c}{\rho_s (1 - \phi_0(x))(k_s + k_c)}$. Then $B_3(x)$ is independent of time t and it's easy to check that $B_2(x, \phi) = B_3(x) \cdot (1 - \phi) \leq B_{30} \cdot (1 - \phi)$.

Applying quadrature rule in [28] to (4.5) with enough algebraic order k, we have

$$
\begin{aligned}
\bar{\phi}_K^{n+1} &= \bar{\phi}_K^n + \triangle t \overline{B_2(\phi^n)c_f} \\
&= \bar{\phi}_K^n + \triangle t \left(\sum_{i=1}^{3} \sum_{\beta=1}^{k+1} \hat{w}_\beta (B_3)_K^{i,\beta} (1 - \phi_K^{i,\beta})(c_f)_K^{i,\beta} + \sum_{\gamma=1}^{L} \hat{w}_\gamma (B_3)_K^\gamma (1 - \phi_K^\gamma)(c_f)_K^\gamma \right) \\
&\geq \bar{\phi}_K^n
\end{aligned}
$$

under the assumption $0 \leq c_f^n \leq 1$ and $\phi_K^n < 1$. Moreover, we have

$$
\begin{aligned}
\bar{\phi}_K^{n+1} &= \bar{\phi}_K^n + \triangle t \left(\sum_{i=1}^{3} \sum_{\beta=1}^{k+1} \hat{w}_\beta (B_3)_K^{i,\beta} (1 - \phi_K^{i,\beta})(c_f)_K^{i,\beta} + \sum_{\gamma=1}^{L} \hat{w}_\gamma (B_3)_K^\gamma (1 - \phi_K^\gamma)(c_f)_K^\gamma \right) \\
&\leq \bar{\phi}_K^n + \triangle t \left(\sum_{i=1}^{3} \sum_{\beta=1}^{k+1} \hat{w}_\beta (B_3)_K^{i,\beta} (1 - \phi_K^{i,\beta}) + \sum_{\gamma=1}^{L} \hat{w}_\gamma (B_3)_K^\gamma (1 - \phi_K^\gamma) \right) \\
&\leq \bar{\phi}_K^n + \triangle t \left(\sum_{i=1}^{3} \sum_{\beta=1}^{k+1} \hat{w}_\beta B_{30} (1 - \phi_K^{i,\beta}) + \sum_{\gamma=1}^{L} \hat{w}_\gamma B_{30} (1 - \phi_K^\gamma) \right) \\
&= \bar{\phi}_K^n + \triangle t B_{30} \left(\sum_{i=1}^{3} \sum_{\beta=1}^{k+1} \hat{w}_\beta (1 - \phi_K^{i,\beta}) + \sum_{\gamma=1}^{L} \hat{w}_\gamma (1 - \phi_K^\gamma) \right) \\
&= \bar{\phi}_K^n + \triangle t B_{30} (1 - \bar{\phi}_K^n).
\end{aligned}
$$

Thus $\bar{\phi}_K^{n+1} < 1$ under the condition (4.6). $\square$

The bound-preserving property for $\bar{r}_K^{n+1}$ is relatively difficult to derive. Therefore, instead of obtaining $0 \leq \bar{r}_K^{n+1} \leq \bar{\phi}_K^{n+1}$ directly, we apply the positivity-preserving technique to $\bar{r}_K^{n+1}$ and $\bar{r}_{2K}^{n+1}$ in (4.2) and (4.4), respectively, which further yields $0 \leq \bar{r}_K^{n+1} \leq \bar{\phi}_K^{n+1}$ due to the fact that $\bar{r}_K^{n+1} + \bar{r}_{2K}^{n+1} = \bar{\phi}_K^{n+1}$. To construct the positivity-preserving technique, in (4.2), we take $\xi = 1$ in K to obtain the equation satisfied by the cell average of r

$$
\bar{r}_K^{n+1} = H_K^c(r, c_f, \boldsymbol{u}) + H_K^d(r, c_f, \boldsymbol{u}, \phi) + H_K^s(r, c_f, c_I, f_P, f_I, \phi), \tag{4.7}
$$

where

$$
H_K^c(r, c_f, \boldsymbol{u}) = \frac{1}{3} \bar{r}_K^n - \lambda \sum_{i=1}^{3} \int_{e_K^i} \widehat{\boldsymbol{u}c_f} \cdot \boldsymbol{\nu}_K^i ds, \tag{4.8}
$$

$$
H_K^d(r, c_f, \boldsymbol{u}, \phi) = \frac{1}{3} \bar{r}_K^n + \lambda \sum_{i=1}^{3} \int_{e_K^i} \left(\{ \boldsymbol{D}(\boldsymbol{u}) \nabla c \} \cdot \boldsymbol{\nu}_K^i + \frac{\tilde{\alpha}}{\ell_K^i} [c] \mathbf{n}_e \cdot \boldsymbol{\nu}_K^i \right) ds, \tag{4.9}
$$

$$
H_K^s(r, c_f, c_I, f_P, f_I, \phi) = \frac{1}{3} \bar{r}_K^n + \triangle t \overline{f_I c_I - f_P c_f - B_1(\phi) c_f}, \tag{4.10}
$$

with $\lambda = \frac{\triangle t}{|K|}$ being the ratio of time step and area of triangular element K, and $\overline{f_P c_f - f_I c_I - B_1(\phi) c_f}$ being the cell average of $f_P c_f - f_I c_I - B_1(\phi) c_f$ on K. We will demonstrate the positivity-preserving property for $\bar{r}_K^{n+1}$ by collecting the following three lemmas.

Lemma 4.2. *Given $r^n > 0$ ($c_f^n > 0$), we have $H_K^s(r, c_f, c_I, f_P, f_I, \phi) > 0$, if the time step satisfies*

$$\triangle t \le \frac{\phi_\star}{6 f_{PM}}, \quad \triangle t \le \frac{\phi_\star}{6 B_1(\phi_\star)}, \tag{4.11}$$

where

$$f_{PM} = \max_{i, \beta, \gamma} \{ (f_P)_K^{i,\beta}, (f_P)_K^{\gamma} \}.$$

Proof. We can split (4.10) as

$$H_K^s = \triangle t \overline{f_I c_I} + \left(\frac{1}{6} \bar{r}_K^n - \triangle t \overline{f_P c_f} \right) + \left(\frac{1}{6} \bar{r}_K^n - \triangle t \overline{B_1(\phi) c_f} \right) := L_1 + L_2 + L_3.$$

It is easy to check that $L_1 = \triangle t \overline{f_I c_I} \ge 0$. We only need to consider L_2 and L_3. Applying quadrature rule in [28] with enough algebraic order k to L_2 and L_3, respectively, we can get

$$
\begin{aligned}
L_2 &= \frac{1}{6} \bar{r}_K^n - \triangle t \overline{f_P c_f} \\
&= \frac{1}{6} \left(\sum_{i=1}^{3} \sum_{\beta=1}^{k+1} \tilde{w}_\beta r_K^{i,\beta} + \sum_{\gamma=1}^{L} \hat{w}_\gamma r_K^\gamma \right) - \triangle t \left(\sum_{i=1}^{3} \sum_{\beta=1}^{k+1} \tilde{w}_\beta (f_P)_K^{i,\beta} (c_f)_K^{i,\beta} + \sum_{\gamma=1}^{L} \hat{w}_\gamma (f_P)_K^\gamma (c_f)_K^\gamma \right) \\
&= \sum_{i=1}^{3} \sum_{\beta=1}^{k+1} \tilde{w}_\beta \left(\frac{1}{6} r_K^{i,\beta} - \triangle t (f_P)_K^{i,\beta} (c_f)_K^{i,\beta} \right) + \sum_{\gamma=1}^{L} \hat{w}_\gamma \left(\frac{1}{6} r_K^\gamma - \triangle t (f_P)_K^\gamma (c_f)_K^\gamma \right) \\
&\ge \sum_{i=1}^{3} \sum_{\beta=1}^{k+1} \tilde{w}_\beta \left(\frac{1}{6} r_K^{i,\beta} - \triangle t (f_P)_K^{i,\beta} r_K^{i,\beta} \phi_\star^{-1} \right) + \sum_{\gamma=1}^{L} \hat{w}_\gamma \left(\frac{1}{6} r_K^\gamma - \triangle t (f_P)_K^\gamma r_K^\gamma \phi_\star^{-1} \right) \\
&= \sum_{i=1}^{3} \sum_{\beta=1}^{k+1} \tilde{w}_\beta \left(\frac{1}{6} - \triangle t (f_P)_K^{i,\beta} \phi_\star^{-1} \right) r_K^{i,\beta} + \sum_{\gamma=1}^{L} \hat{w}_\gamma \left(\frac{1}{6} - \triangle t (f_P)_K^\gamma \phi_\star^{-1} \right) r_K^\gamma.
\end{aligned}
$$

Thus $L_2 > 0$ under the condition (4.11).

$$
\begin{aligned}
L_3 &= \frac{1}{6} \bar{r}_K^n - \triangle t \overline{B_1(\phi) c_f} \\
&= \frac{1}{6} \left(\sum_{i=1}^{3} \sum_{\beta=1}^{k+1} \tilde{w}_\beta r_K^{i,\beta} + \sum_{\gamma=1}^{L} \hat{w}_\gamma r_K^\gamma \right) - \triangle t \left(\sum_{i=1}^{3} \sum_{\beta=1}^{k+1} \tilde{w}_\beta B_1(\phi_K^{i,\beta}) (c_f)_K^{i,\beta} + \sum_{\gamma=1}^{L} \hat{w}_\gamma B_1(\phi_K^\gamma) (c_f)_K^\gamma \right) \\
&= \sum_{i=1}^{3} \sum_{\beta=1}^{k+1} \tilde{w}_\beta \left(\frac{1}{6} r_K^{i,\beta} - \triangle t B_1(\phi_K^{i,\beta}) (c_f)_K^{i,\beta} \right) + \sum_{\gamma=1}^{L} \hat{w}_\gamma \left(\frac{1}{6} r_K^\gamma - \triangle t B_1(\phi_K^\gamma) (c_f)_K^\gamma \right) \\
&\ge \sum_{i=1}^{3} \sum_{\beta=1}^{k+1} \tilde{w}_\beta \left(\frac{1}{6} r_K^{i,\beta} - \triangle t B_1(\phi_K^{i,\beta}) r_K^{i,\beta} \phi_\star^{-1} \right) + \sum_{\gamma=1}^{L} \hat{w}_\gamma \left(\frac{1}{6} r_K^\gamma - \triangle t B_1(\phi_K^\gamma) r_K^\gamma \phi_\star^{-1} \right) \\
&= \sum_{i=1}^{3} \sum_{\beta=1}^{k+1} \tilde{w}_\beta \left(\frac{1}{6} - \triangle t B_1(\phi_K^{i,\beta}) \phi_\star^{-1} \right) r_K^{i,\beta} + \sum_{\gamma=1}^{L} \hat{w}_\gamma \left(\frac{1}{6} - \triangle t B_1(\phi_K^\gamma) \phi_\star^{-1} \right) r_K^\gamma \\
&\ge \sum_{i=1}^{3} \sum_{\beta=1}^{k+1} \tilde{w}_\beta \left(\frac{1}{6} - \triangle t B_1(\phi_\star) \phi_\star^{-1} \right) r_K^{i,\beta} + \sum_{\gamma=1}^{L} \hat{w}_\gamma \left(\frac{1}{6} - \triangle t B_1(\phi_\star) \phi_\star^{-1} \right) r_K^\gamma.
\end{aligned}
$$

Thus $L_3 > 0$ under the condition (4.11). To sum up, $H_K^s(r, c_f, c_I, f_P, f_I, \phi) = L_1 + L_2 + L_3 > 0$ under the condition (4.11). $\square$

9

In the following two lemmas, we only consider second order scheme, i.e. we use P^1 element, and apply quadrature rule in [28] with $k = 1$ in cell and the the corresponding 2 point Gaussian quadrature rule on cell interface. Note that in this case, $\hat{\omega}_\beta = \frac{1}{3}\omega_\beta$.

Lemma 4.3. *Given $r^n > 0$ ($c_f^n > 0$), we have $H_K^c(r, c_f, \boldsymbol{u}) > 0$, if α satisfies*

$$\alpha \geq \max_{i,\beta,K}\{|\boldsymbol{u}_K^{i,\beta}|\}, \tag{4.12}$$

and the time step satisfies

$$\triangle t \leq \min_{i,\beta,m}\{\frac{|K|\phi(V_m)}{9\ell_K^i(|\boldsymbol{u}_K^{i,\beta}| + \alpha)}\}, \tag{4.13}$$

where $\phi(V_m)$, $m = 1, 2, 3$ are the values of ϕ at vertices $V_m \in K$ at time level n.

Proof. Applying quadrature rule for $k = 1$, we can rewrite (4.8) as

$$H_K^c = \frac{1}{3}\bar{r}_K^n - \lambda \sum_{i=1}^3 \int_{e_K^i} \widehat{\boldsymbol{u}c_f} \cdot \boldsymbol{\nu}_K^i ds$$

$$= \frac{1}{9}\left(\sum_{i=1}^3 \sum_{\beta=1}^2 w_\beta r_K^{i,\beta}\right) - \lambda \sum_{i=1}^3 \sum_{\beta=1}^2 w_\beta \ell_K^i (\widehat{\boldsymbol{u}c_f})_{e_K^i}^{i,\beta} \cdot \boldsymbol{\nu}_K^i$$

$$= \sum_{i=1}^3 \sum_{\beta=1}^2 w_\beta \left(\frac{1}{9}r_K^{i,\beta} - \lambda\ell_K^i (\widehat{\boldsymbol{u}c_f})_{e_K^i}^{i,\beta} \cdot \boldsymbol{\nu}_K^i\right)$$

$$= \sum_{i=1}^3 \sum_{\beta=1}^2 w_\beta \left(\frac{1}{9}r_K^{i,\beta} - \lambda\ell_K^i \left(\frac{1}{2}\boldsymbol{u}_{K_i}^{i,\beta} \cdot \boldsymbol{\nu}_K^i (c_f)_{K_i}^{i,\beta} + \frac{1}{2}\boldsymbol{u}_K^{i,\beta} \cdot \boldsymbol{\nu}_K^i (c_f)_K^{i,\beta} - \alpha(c_f)_{K_i}^{i,\beta} + \alpha(c_f)_K^{i,\beta}\right)\right)$$

$$= \sum_{i=1}^3 \sum_{\beta=1}^2 w_\beta \left\{\left(\frac{1}{18}r_K^{i,\beta} - \frac{1}{2}\lambda\ell_K^i \left(\boldsymbol{u}_{K_i}^{i,\beta} \cdot \boldsymbol{\nu}_K^i (c_f)_{K_i}^{i,\beta} - \alpha(c_f)_{K_i}^{i,\beta} + \alpha(c_f)_K^{i,\beta}\right)\right)\right.$$

$$\left. + \left(\frac{1}{18}r_K^{i,\beta} - \frac{1}{2}\lambda\ell_K^i \left(\boldsymbol{u}_K^{i,\beta} \cdot \boldsymbol{\nu}_K^i (c_f)_K^{i,\beta} - \alpha(c_f)_K^{i,\beta} + \alpha(c_f)_K^{i,\beta}\right)\right)\right\}$$

$$:= \sum_{i=1}^3 \sum_{\beta=1}^2 w_\beta \left(L_1^{i,\beta} + L_2^{i,\beta}\right).$$

Since c_f and r are both approximated by linear functions, they can be represented as a linear combination of their values on three vertices $\{V_1, V_2, V_3\}$ of K, i.e. for any point $x_K^\rho \in K$,

$$(c_f)_K^\rho = \sum_{m=1}^3 \mu_m^\rho c_f(V_m), \quad r_K^\rho = \sum_{m=1}^3 \mu_m^\rho r(V_m) = \sum_{m=1}^3 \mu_m^\rho \phi(V_m)c_f(V_m), \tag{4.14}$$

where $0 \leq \mu_1^\rho, \mu_2^\rho, \mu_3^\rho \leq 1$ and $\mu_1^\rho + \mu_2^\rho + \mu_3^\rho = 1$ are the barycentric coordinates of x_K^ρ in K. Then we have

$$L_1^{i,\beta} = \frac{1}{18}r_K^{i,\beta} - \frac{1}{2}\lambda\ell_K^i \left(\boldsymbol{u}_{K_i}^{i,\beta} \cdot \boldsymbol{\nu}_K^i (c_f)_{K_i}^{i,\beta} - \alpha(c_f)_{K_i}^{i,\beta} + \alpha(c_f)_K^{i,\beta}\right)$$

$$= \sum_{m=1}^3 \frac{1}{18}\mu_m^{i,\beta}\phi(V_m)c_f(V_m) - \frac{1}{2}\lambda\ell_K^i \left(\boldsymbol{u}_{K_i}^{i,\beta} \cdot \boldsymbol{\nu}_K^i (c_f)_{K_i}^{i,\beta} - \alpha(c_f)_{K_i}^{i,\beta} + \alpha\sum_{m=1}^3 \mu_m^{i,\beta}c_f(V_m)\right)$$

$$= \sum_{m=1}^3 \mu_m^{i,\beta}\left(\frac{1}{18}\phi(V_m) - \frac{1}{2}\lambda\ell_K^i\alpha\right)c_f(V_m) + \frac{1}{2}\lambda\ell_K^i(\alpha - \boldsymbol{u}_{K_i}^{i,\beta} \cdot \boldsymbol{\nu}_K^i)(c_f)_{K_i}^{i,\beta},$$

10

and

$$L_2^{i,\beta} = \frac{1}{18}r_K^{i,\beta} - \frac{1}{2}\lambda\ell_K^i\left(\boldsymbol{u}_K^{i,\beta}\cdot\boldsymbol{\nu}_K^i(c_f)_K^{i,\beta} - \alpha(c_f)_{K_i}^{i,\beta} + \alpha(c_f)_K^{i,\beta}\right)$$

$$= \sum_{m=1}^{3}\frac{1}{18}\mu_m^{i,\beta}\phi(V_m)c_f(V_m) - \frac{1}{2}\lambda\ell_K^i\left(\boldsymbol{u}_K^{i,\beta}\cdot\boldsymbol{\nu}_K^i\sum_{m=1}^{3}\mu_m^{i,\beta}c_f(V_m) - \alpha(c_f)_{K_i}^{i,\beta} + \alpha\sum_{m=1}^{3}\mu_m^{i,\beta}c_f(V_m)\right)$$

$$= \sum_{m=1}^{3}\mu_m^{i,\beta}\left(\frac{1}{18}\phi(V_m) - \frac{1}{2}\lambda\ell_K^i(\boldsymbol{u}_K^{i,\beta}\cdot\boldsymbol{\nu}_K^i + \alpha)\right)c_f(V_m) + \frac{1}{2}\lambda\ell_K^i\alpha(c_f)_{K_i}^{i,\beta}.$$

Therefore $L_1^{i,\beta}, L_2^{i,\beta} > 0$ under the conditions (4.12) and (4.13), respectively, which further yields $H_K^c > 0$. $\square$

Lemma 4.4. *Given $r^n > 0$ ($c_f^n > 0$), we have $H_K^d(r, c_f, \boldsymbol{u}, \phi) > 0$, if $\tilde{\alpha}$ satisfies*

$$\tilde{\alpha} \geq \frac{(3+\sqrt{3})\Lambda}{2\rho}, \tag{4.15}$$

and the time step satisfies

$$\Delta t \leq \min_m\{\frac{|K|\phi(V_m)}{18\tilde{\alpha}}\}, \quad \Delta t \leq \min_m\{\frac{\rho|K|\phi(V_m)}{27(3+\sqrt{3})\Lambda}\}, \tag{4.16}$$

where $\phi(V_m)$, $m = 1, 2, 3$ are the values of ϕ at the vertices $V_m \in K$ at time level n, ρ is the parameter used in the definition of regularity of Ω_h, and Λ is the largest spectral radius of $\mathbf{D}$ in K's.

Proof. For the diffusion part

$$H_K^d(r, c_f, \boldsymbol{u}, \phi) = \frac{1}{3}\bar{r}_K^n + \lambda\sum_{i=1}^{3}\int_{e_K^i}\left(\{\boldsymbol{D}(\boldsymbol{u})\nabla c_f\}\cdot\boldsymbol{\nu}_K^i + \frac{\tilde{\alpha}}{\ell_K^i}[c_f]\mathbf{n}_e\cdot\boldsymbol{\nu}_K^i\right)ds.$$

Since $\boldsymbol{D}$ is symmetric, following [32], we can rewrite the diffusion term as a directional derivative

$$\boldsymbol{D}\nabla c_f\cdot\boldsymbol{\nu}_K^i = \boldsymbol{D}\boldsymbol{\nu}_K^i\cdot\nabla c_f = S^i\frac{\partial c_f}{\partial \boldsymbol{l}^i},$$

where $S^i = \|\boldsymbol{D}\boldsymbol{\nu}_K^i\| \leq \Lambda$ and $\boldsymbol{l}^i = \boldsymbol{D}\boldsymbol{\nu}_K^i/\|\boldsymbol{D}\boldsymbol{\nu}_K^i\|$. Define $S_K^i = S^i|_K$, $S_{K_i}^i = S^i|_{K_i}$ and $\boldsymbol{l}_K^i = \boldsymbol{l}^i|_K$, $\boldsymbol{l}_{K_i}^i = \boldsymbol{l}^i|_{K_i}$. For each quadrature point $x_K^{i,\beta}$ on the edge e_K^i, we can find the corresponding points $\tilde{x}_K^{i,\beta} \in \partial K$ and $\tilde{x}_{K_i}^{i,\beta} \in \partial K_i$ such that $\overrightarrow{\tilde{x}_K^{i,\beta}x_K^{i,\beta}}$ and $\overrightarrow{x_K^{i,\beta}\tilde{x}_{K_i}^{i,\beta}}$ are the same direction with $\boldsymbol{l}_K^i$ and $\boldsymbol{l}_{K_i}^i$, respectively. See Figure 2 for an illustration. At the quadrature point $x = x_K^{i,\beta}$, we have

$$\{\boldsymbol{D}(\boldsymbol{u})\nabla c_f\}_{e_K^i}^{i,\beta}\cdot\boldsymbol{\nu}_K^i = \frac{1}{2}\boldsymbol{D}(\boldsymbol{u}_K^{i,\beta})\nabla(c_f)_K^{i,\beta}\cdot\boldsymbol{\nu}_K^i + \frac{1}{2}\boldsymbol{D}(\boldsymbol{u}_{K_i}^{i,\beta})\nabla(c_f)_{K_i}^{i,\beta}\cdot\boldsymbol{\nu}_K^i$$

$$= \frac{1}{2}S_K^{i,\beta}\frac{(c_f)_K^{i,\beta} - c_f(\tilde{x}_K^{i,\beta})}{\|x_K^{i,\beta} - \tilde{x}_K^{i,\beta}\|} + \frac{1}{2}S_{K_i}^{i,\beta}\frac{c_f(\tilde{x}_{K_i}^{i,\beta}) - (c_f)_{K_i}^{i,\beta}}{\|\tilde{x}_{K_i}^{i,\beta} - x_K^{i,\beta}\|}$$

$$= \frac{S_K^{i,\beta}}{2\|x_K^{i,\beta} - \tilde{x}_K^{i,\beta}\|}(c_f)_K^{i,\beta} - \frac{S_{K_i}^{i,\beta}}{2\|\tilde{x}_{K_i}^{i,\beta} - x_K^{i,\beta}\|}(c_f)_{K_i}^{i,\beta} - \frac{S_K^{i,\beta}}{2\|x_K^{i,\beta} - \tilde{x}_K^{i,\beta}\|}c_f(\tilde{x}_K^{i,\beta}) + \frac{S_{K_i}^{i,\beta}}{2\|\tilde{x}_{K_i}^{i,\beta} - x_K^{i,\beta}\|}c_f(\tilde{x}_{K_i}^{i,\beta}).$$

Figure 2: The points chosen to evaluate directional derivative in the diffusion part.

Therefore, we can rewrite $H_K^d(r, c_f, \boldsymbol{u}, \phi)$ as

$$
\begin{aligned}
H_K^d &= \frac{1}{6}\bar{r}_K^n + \frac{1}{6}\bar{r}_K^n + \lambda \sum_{i=1}^{3} \int_{e_K^i} \left(\{\boldsymbol{D}(\boldsymbol{u})\nabla c_f\} \cdot \boldsymbol{\nu}_K^i + \frac{\tilde{\alpha}}{\ell_K^i}[c_f]\mathbf{n}_e \cdot \boldsymbol{\nu}_K^i \right) ds \\
&= \frac{1}{6}\bar{r}_K^n + \frac{1}{18}\sum_{i=1}^{3}\sum_{\beta=1}^{2} w_\beta r_K^{i,\beta} + \lambda \sum_{i=1}^{3}\sum_{\beta=1}^{2} w_\beta \ell_K^i \left(\{\boldsymbol{D}(\boldsymbol{u})\nabla c_f\}_{e_K^i}^{i,\beta} \cdot \boldsymbol{\nu}_K^i + \frac{\tilde{\alpha}}{\ell_K^i}(c_f)_{K_i}^{i,\beta} - \frac{\tilde{\alpha}}{\ell_K^i}(c_f)_{K}^{i,\beta} \right) \\
&= \frac{1}{6}\bar{r}_K^n + \frac{1}{18}\sum_{i=1}^{3}\sum_{\beta=1}^{2}\sum_{m=1}^{3} w_\beta \mu_m^{i,\beta} \phi(V_m) c_f(V_m) + \lambda \sum_{i=1}^{3}\sum_{\beta=1}^{2} w_\beta \ell_K^i \left(\{\boldsymbol{D}(\boldsymbol{u})\nabla c_f\}_{e_K^i}^{i,\beta} \cdot \boldsymbol{\nu}_K^i + \frac{\tilde{\alpha}}{\ell_K^i}(c_f)_{K_i}^{i,\beta} - \frac{\tilde{\alpha}}{\ell_K^i}(c_f)_{K}^{i,\beta} \right) \\
&= \frac{1}{6}\bar{r}_K^n + \sum_{i=1}^{3}\sum_{\beta=1}^{2} w_\beta \left(\frac{1}{18}\sum_{m=1}^{3} \mu_m^{i,\beta} \phi(V_m) c_f(V_m) + \lambda \ell_K^i \left(\{\boldsymbol{D}(\boldsymbol{u})\nabla c_f\}_{e_K^i}^{i,\beta} \cdot \boldsymbol{\nu}_K^i + \frac{\tilde{\alpha}}{\ell_K^i}(c_f)_{K_i}^{i,\beta} - \frac{\tilde{\alpha}}{\ell_K^i}(c_f)_{K}^{i,\beta} \right) \right) \\
&:= \sum_{i=1}^{3}\sum_{\beta=1}^{2} w_\beta L_1^{i,\beta} + L_2,
\end{aligned}
$$

where

$$
\begin{aligned}
L_1^{i,\beta} &= \frac{1}{18}\sum_{m=1}^{3} \mu_m^{i,\beta} \phi(V_m) c_f(V_m) + \lambda \ell_K^i \left[\left(\frac{S_K^{i,\beta}}{2\|x_K^{i,\beta} - \tilde{x}_K^{i,\beta}\|} - \frac{\tilde{\alpha}}{\ell_K^i} \right)(c_f)_K^{i,\beta} + \left(\frac{\tilde{\alpha}}{\ell_K^i} - \frac{S_{K_i}^{i,\beta}}{2\|\tilde{x}_{K_i}^{i,\beta} - x_K^{i,\beta}\|} \right)(c_f)_{K_i}^{i,\beta} \right. \\
&\quad \left. + \frac{S_{K_i}^{i,\beta}}{2\|\tilde{x}_{K_i}^{i,\beta} - x_K^{i,\beta}\|} c_f(\tilde{x}_{K_i}^{i,\beta}) \right], \\
L_2 &= \frac{1}{6}\bar{r}_K^n - \lambda \ell_K^i \sum_{i=1}^{3}\sum_{\beta=1}^{2} \frac{\omega_\beta S_K^{i,\beta}}{2\|x_K^{i,\beta} - \tilde{x}_K^{i,\beta}\|} c_f(\tilde{x}_K^{i,\beta}).
\end{aligned}
$$
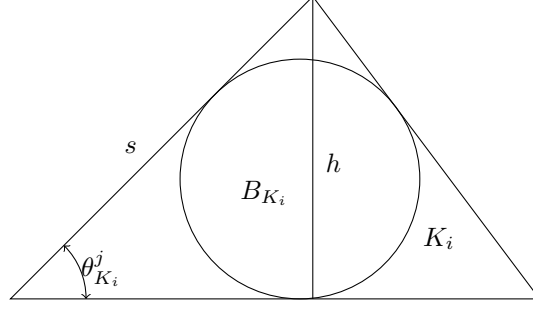
Figure 3: Triangle K_i and its sine

We need to make $L_1^{i,\beta}, L_2 > 0$. In fact

$$
\begin{aligned}
L_1^{i,\beta} =& \frac{1}{18}\sum_{m=1}^{3}\mu_m^{i,\beta}\phi(V_m)c_f(V_m) + \lambda\ell_K^i\left(\frac{S_K^{i,\beta}}{2\|x_K^{i,\beta} - \tilde{x}_K^{i,\beta}\|} - \frac{\tilde{\alpha}}{\ell_K^i}\right)(c_f)_K^{i,\beta} \\
& + \lambda\ell_K^i\left(\frac{\tilde{\alpha}}{\ell_K^i} - \frac{S_{K_i}^{i,\beta}}{2\|\tilde{x}_{K_i}^{i,\beta} - x_K^{i,\beta}\|}\right)(c_f)_{K_i}^{i,\beta} + \lambda\ell_K^i\frac{S_{K_i}^{i,\beta}}{2\|\tilde{x}_{K_i}^{i,\beta} - x_K^{i,\beta}\|}c_f(\tilde{x}_{K_i}^{i,\beta}) \\
=& \sum_{m=1}^{3}\mu_m^{i,\beta}\left(\frac{1}{18}\phi(V_m) + \lambda\ell_K^i\left(\frac{S_K^{i,\beta}}{2\|x_K^{i,\beta} - \tilde{x}_K^{i,\beta}\|} - \frac{\tilde{\alpha}}{\ell_K^i}\right)\right)c_f(V_m) \\
& + \lambda\ell_K^i\left(\frac{\tilde{\alpha}}{\ell_K^i} - \frac{S_{K_i}^{i,\beta}}{2\|\tilde{x}_{K_i}^{i,\beta} - x_K^{i,\beta}\|}\right)(c_f)_{K_i}^{i,\beta} + \lambda\ell_K^i\frac{S_{K_i}^{i,\beta}}{2\|\tilde{x}_{K_i}^{i,\beta} - x_K^{i,\beta}\|}c_f(\tilde{x}_{K_i}^{i,\beta}).
\end{aligned}
$$

Since $S_K^{i,\beta}, S_{K_i}^{i,\beta} \leq \Lambda$, to make $L_1^{i,\beta} > 0$, we need

$$
\tilde{\alpha} \geq \frac{\ell_K^i\Lambda}{2\|\tilde{x}_{K_i}^{i,\beta} - x_K^{i,\beta}\|}, \quad \lambda\ell_K^i\left(\frac{\tilde{\alpha}}{\ell_K^i} - \frac{S_K^{i,\beta}}{2\|x_K^{i,\beta} - \tilde{x}_K^{i,\beta}\|}\right) \leq \frac{1}{18}\phi(V_m).
$$

It's easy to compute that

$$
\frac{\ell_K^i}{\|\tilde{x}_{K_i}^{i,\beta} - x_K^{i,\beta}\|} \leq \frac{3 + \sqrt{3}}{\min_j \sin\left(\theta_{K_i}^j\right)},
$$

where the $\theta_{K_i}^j$ is the angle in triangle K_i which is opposite to the edge $e_{K_i}^j$. From Figure 3 and regularity assumption of Ω_h, for all angle $\theta_{K_i}^j$ in K_i, we have

$$
\sin\theta_{K_i}^j = \frac{h}{s} \geq \frac{\text{diam}(B_{K_i})}{\text{diam}(K_i)} \geq \rho.
$$

Therefore $L_1^{i,\beta} > 0$ under the conditions (4.15) and (4.16). As for L_2, similar to (4.14), we write

$$
c_f(\tilde{x}_K^{i,\beta}) = \sum_{m=1}^{3}\tilde{\mu}_m^{i,\beta}c_f(V_m),
$$

with $0 \leq \tilde{\mu}_m^{i,\beta} \leq 1$ and $\sum\limits_{m=1}^{3} \tilde{\mu}_m^{i,\beta} = 1$, and use the fact that $\omega_1 = \omega_2 = \frac{1}{2}$. Then

$$
\begin{aligned}
L_2 =& \frac{1}{6}\bar{r}_K^n - \lambda \ell_K^i \sum_{i=1}^{3} \sum_{\beta=1}^{2} \sum_{m=1}^{3} \frac{\tilde{\mu}_m^{i,\beta} S_K^{i,\beta}}{4\|x_K^{i,\beta} - \tilde{x}_K^{i,\beta}\|} c_f(V_m) \\
=& \sum_{m=1}^{3} \left(\frac{1}{18}\phi(V_m) - \lambda \ell_K^i \sum_{i=1}^{3} \sum_{\beta=1}^{2} \frac{\tilde{\mu}_m^{i,\beta} S_K^{i,\beta}}{4\|x_K^{i,\beta} - \tilde{x}_K^{i,\beta}\|} \right) c_f(V_m) \\
\geq& \sum_{m=1}^{3} \left(\frac{1}{18}\phi(V_m) - \lambda \sum_{i=1}^{3} \sum_{\beta=1}^{2} \frac{(3+\sqrt{3})\Lambda}{4\rho} \right) c_f(V_m) \\
=& \sum_{m=1}^{3} \left(\frac{1}{18}\phi(V_m) - \lambda \frac{3(3+\sqrt{3})\Lambda}{2\rho} \right) c_f(V_m).
\end{aligned}
$$

Thus, $L_2 > 0$ under the condition (4.16). Therefore we have $H_K^d(r, c_f, \boldsymbol{u}, \phi) > 0$ under the conditions (4.15) and (4.16). $\qquad\square$

Collecting the three lemmas above, we have the following Lemma:

Lemma 4.5. *Given $r^n > 0$, and the parameters α and $\tilde{\alpha}$ satisfy (4.12) and (4.15), respectively. Then $\bar{r}_K^{n+1} > 0$ under the conditions (4.11), (4.13) and (4.16).*

Compare the equation (4.4) with (4.2), we can observe that the equation for r_2 is almost the same as that for r, except that its source term contains a positive term $+B_1(\phi)c_f$ instead of $-B_1(\phi)c_f$, which will benefit its positivity. Therefore, we can get a similar lemma for r_2:

Lemma 4.6. *Given $r_2^n > 0$, and the parameters α and $\tilde{\alpha}$ satisfy (4.12) and (4.15), respectively. Then $\bar{r}_{2K}^{n+1} > 0$ under the conditions (4.11), (4.13) and (4.16).*

Combine Lemmas 4.5, 4.6 and 4.1, and use the fact that $r^n + r_2^n = \phi^n, r^{n+1} + r_2^{n+1} = \phi^{n+1}$, we finally reach our main theorem:

Theorem 4.7. *Given $0 \leq r^n \leq \phi^n < 1$, if we chose consistent flux pair $\hat{\boldsymbol{u}}, \widehat{\boldsymbol{u}c_f}$ and the penalty parameters α and $\tilde{\alpha}$ satisfying (4.12) and (4.15), respectively, then $\bar{\phi}_K^n \leq \bar{\phi}_K^{n+1} < 1$ and $0 \leq \bar{r}_K^{n+1} \leq \bar{\phi}_K^{n+1}$ under the conditions (4.6), (4.11), (4.13), and (4.16).*

5 Bound-preserving technique for high-order schemes

In this section, we proceed to discuss the high-order bound-preserving technique.

5.1 High-order spatial discretization

In Lemmas 4.3 and 4.4, our proofs are based on P^1 elements. To attain high-order accuracy, we use $P^k(k > 2)$ polynomials and apply the flux limiters following [10, 23].

We write (4.7) as

$$\bar{r}_K^{n+1} = \bar{r}_K^n + \lambda \sum_{i=1}^{3} \left(\theta_{e_K^i} \hat{F}_{e_K^i} + (1 - \theta_{e_K^i}) \hat{f}_{e_K^i} \right) + \Delta t \bar{s},$$

where

$$\hat{F}_{e_K^i} = -\int_{e_K^i} \widehat{uc_f} \cdot \nu_i ds + \int_{e_K^i} \left(\{ \boldsymbol{D}(\boldsymbol{u}) \nabla c \} \cdot \nu_K^i + \frac{\tilde{\alpha}}{\ell_K^i} [c_f] \right) ds, \quad \bar{s} = \overline{f_I c_I - f_P c_f - B_1(\phi) c_f} \qquad (5.1)$$

are high-order flux and source, respectively, and $\hat{f}_{e_K^i}$ is the second-order bound-preserving flux analyzed in Section 4. In lemma 4.2, we considered high-order approximations of the source term. Therefore, we only discuss the modification of the high-order fluxes in this section, which is implemented by choosing an appropriate parameter θ_K^i. The cell average can be written as

$$\bar{r}_K^{n+1} = \bar{r}_K^n + \lambda \sum_{i=1}^{3} \hat{f}_{e_K^i} + \lambda \sum_{i=1}^{3} \theta_{e_K^i} (\hat{F}_{e_K^i} - \hat{f}_{e_K^i}) + \Delta t \bar{s} = \bar{r}_L^{n+1} + \lambda \sum_{i=1}^{3} \theta_{e_K^i} (\hat{F}_{e_K^i} - \hat{f}_{e_K^i}),$$

where

$$\bar{r}_L^{n+1} = \bar{r}_K^n + \lambda \sum_{i=1}^{3} \hat{f}_{e_K^i} + \Delta t \bar{s}$$

is the second-order cell average which was proved to be physically relevant if Δt is sufficiently small. To compute $\hat{f}_{e_K^i}$, we replace the high-order c_f in $\hat{F}_{e^i}$ by a second-order approximation $\check{c}_f \in [0,1]$. To construct it, we can simply apply the second-order L^2 projection to the high-order r^n to get $\check{r}_K^n$ and high-order ϕ^n to get $\check{\phi}_K^n$, and then apply the limiter discussed at the end of this section with $k = 1$ to obtain $0 \le \check{r}_K^n \le \check{\phi}_K^n$. The $\check{c}_f$ can be obtained as the linear interpolation of $\frac{r^n}{\phi^n}$ at the three vertices in each cell K. We choose the parameter $\theta_{e_K^i}$ as follows:

1. For any $K \in \Omega_h$, set $\beta_K^1, \beta_K^2 = 0$.

2. For each edge e_K^i, if $\hat{F}_{e_K^i} - \hat{f}_{e_K^i} \le 0$, set $\beta_K^1 = \beta_K^1 + \hat{F}_{e_K^i} - \hat{f}_{e_K^i}$, otherwise set $\beta_K^2 = \beta_K^2 + \hat{F}_{e_K^i} - \hat{f}_{e_K^i}$.

3. Take $\theta_{K,e_K^i} = \min \left\{ -\frac{\bar{r}_L^{n+1}}{\lambda \beta_K^1}, \frac{\bar{\phi}_K^{n+1} - \bar{r}_L^{n+1}}{\lambda \beta_K^2}, 1 \right\}$.

4. For any $e \in \Gamma_0$, we can find $K_1, K_2 \in \Omega_h$ such that $K_1 \cap K_2 = e$. We take $\theta_e = \min\{\theta_{K_1, e_K^i}, \theta_{K_2, e_K^i}\}$.

The above algorithm can guarantee the monotone increasing and bound-preserving properties for the cell averages of ϕ and r: if $0 \le r^n \le \phi^n < 1$, then $\bar{\phi}_K^n \le \bar{\phi}_K^{n+1} < 1$ and $0 \le \bar{r}_K^{n+1} \le \bar{\phi}_K^{n+1}$, under the appropriate penalty parameters $\alpha, \tilde{\alpha}$ and sufficiently small time step $\triangle t$. It remains to use proper slope limiter to modify ϕ_K^{n+1} and r_K^{n+1} such that $\phi_K^n \le \phi_K^{n+1} < 1$ and $0 \le r_K^{n+1} \le \phi_K^{n+1}$ without loss of cell average and accuracy. As discussed in [9], the traditional slope limiter [29] cannot be applied since the bounds of ϕ_K^{n+1}, r_K^{n+1} are not constants but polynomials changing overtime. In this paper, we extend the limiter introduced in [3] and the algorithm can be described as follows: For polynomials $u(x), U(x) \in P^k(K)$ such that $0 \le \bar{u} \le \bar{U}$ and $U_\star \le U(x) \le U^\star$, where $U_\star, U^\star$ are two positive constants. We obtain a modified $\tilde{u}(x)$ in the following way:

1. Define $\hat{S} = \{x \in K : u(x) < 0\}$. Take

$$\hat{u} = u + \theta \left(\frac{\bar{u}}{\bar{U}} U - u \right), \quad \theta = \max_{y \in \hat{S}} \left\{ \frac{-u(y)\bar{U}}{\bar{u} U(y) - u(y)\bar{U}}, 0 \right\}. \qquad (5.2)$$

2. Set $v = U - \hat{u}$, and repeat the above step for v to get $\hat{v}$.

3. Take $\tilde{u} = U - \hat{v}$ as the new approximation for $u(x)$.

This limiter is proved in [3] to have the following three necessary properties:

- boundness: $0 \leq \tilde{u}(x) \leq U(x), \forall x \in K$,

- average: $\int_K \tilde{u}dx = \int_K udx$,

- accuracy: $\|u(x) - \tilde{u}(x)\|_\infty \leq Ch^{k+1}, h = \text{diam}(K)$.

We use such a slope limiter in the following way: To obtain $\phi_K^n \leq \tilde{\phi}_K^{n+1} < 1$, we take $u = \phi_K^{n+1} - \phi_K^n$ and $U = 1 - \phi_K^n$ in the limiter, and then $\tilde{\phi}_K^{n+1} = \tilde{u} + \phi_K^n$; To obtain $0 \leq \tilde{r}_K^{n+1} \leq \tilde{\phi}_K^{n+1}$, we take $u = r_K^{n+1}$ and $U = \tilde{\phi}_K^{n+1}$ to apply this limiter directly.

5.2   High-order time discretization

In the previous subsection, we only discussed the bound-preserving technique based on Euler forward time discretization. The technique can be extended to high-order time integrations that are convex combinations of Euler forwards. In this paper, we use third-order strong stability preserving (SSP) time discretization to solve the ODE system $\mathbf{u_t} = \mathbf{L(u)}$:

$$\mathbf{u}^{(1)} = \mathbf{u}^n + \Delta t \mathbf{L}(\mathbf{u}, t^n),$$
$$\mathbf{u}^{(2)} = \frac{3}{4}\mathbf{u}^n + \frac{1}{4}\left(\mathbf{u}^{(1)} + \Delta t \mathbf{L}(\mathbf{u}^{(1)}, t^{n+1})\right),$$
$$\mathbf{u}^{n+1} = \frac{1}{3}\mathbf{u}^n + \frac{2}{3}\left(\mathbf{u}^{(2)} + \Delta t \mathbf{L}(\mathbf{u}^{(2)}, t^n + \frac{\Delta t}{2})\right).$$

Another choice is to use third-order SSP multi-step method which is also a convex combination of forward Euler:

$$\mathbf{u}^{n+1} = \frac{16}{27}(\mathbf{u}^n + 3\Delta t \mathbf{L}(\mathbf{u}^n, t^n)) + \frac{11}{27}(\mathbf{u}^{n-3} + \frac{12}{11}\Delta t \mathbf{L}(\mathbf{u}^{n-3}, t^{n-3})).$$

More details can be found in [6, 7, 18].

6   Numerical experiments

In this section, we provide numerical experiments to show the performance of the high-order bound-preserving DG scheme. In all the examples, we use third-order SSP Runge-Kutta discretization in time and P^2 element in space unless otherwise stated. To construct Ω_h, for simplicity, we first equally divide Ω into $N \times N$ rectangles and then obtain a uniform triangular mesh by equally dividing every rectangle into two. See Figure 4 for an illustration. However, the algorithms can be applied for any unstructured triangular meshes.

Example 6.1. *We first test the accuracy of the high-order bound-preserving DG scheme. Because of the restriction $0 \leq c_I \leq 1$, $f = f_I - f_P$ and $f_I, f_P \geq 0$ of right hand side, it's difficult to find a suitable exact*
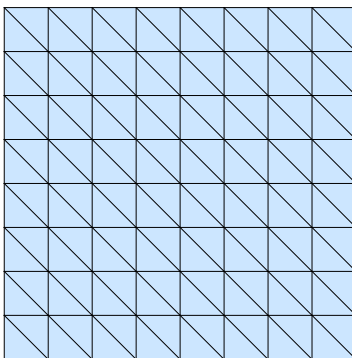
Figure 4: Triangular mesh ($N = 8$)

solution. *Therefore, we use periodic boundary condition and predetermine the Darcy's velocity* $u = (1,1)^T$ *in order to use spectral method to give a reference solution. Initial conditions are given as*

$$c_f(x, y, 0) = 0.5 + 0.5 \cos(x) \cos(y) \qquad \phi(x, y, 0) = 0.5 + 0.4 \sin(x) \sin(y),$$

The source functions are taken as

$$f_I = 2\phi_t, \quad f_P = -\phi_t, \quad c_I = 1,$$

where ϕ_t *is obtained in the computation. The parameters are taken as:*

$$D = 0.1\|\mathbf{u}\|, \qquad k_c = k_s = a_0 = \frac{\alpha}{\rho_s} = 1$$

We use the uniform triangular meshes with $N = 4, 8, 16, 32, 64$, respectively, over the computational domain $\Omega = [0, 2\pi] \times [0, 2\pi]$ and set $\Delta t = 0.001h^2$ to reduce the time error. Moreover, the reference solution is obtained by spectral method on 64×64 equispaced grid points with fourth-order Runge–Kutta time discretization. The computational results at $T = 0.01$ are shown in Table 1, illustrating the error and convergence order of c_f and ϕ, with and without bound-preserving technique respectively. From the table, we can observe optimal convergence rates. Therefore, the flux limiter and slope limiter do not degenerate the convergence order.

Example 6.2. *We take the initial conditions with large gradients*

$$c_f(x, y, 0) = \frac{\text{sign}(\sin(2x) \sin(2y)) + 1}{2}, \quad \phi(x, y, 0) = 0.9 \frac{\text{sign}(\sin(x) \sin(y)) + 1}{2} + 0.05.$$

The source functions are taken as

$$f_I = (1 + \frac{\pi^2}{2} \bar{\phi}_t) \max\{\sin(2x) \sin(2y), 0\}, \quad f_P = -\min\{\sin(2x) \sin(2y), 0\}, \quad c_I = 0,$$

where $\bar{\phi}_t$ *is the average of* ϕ_t *over the whole computational domain. Other parameters are chosen as*

$$\mu = k_0 = k_s = k_c = 1, \quad a_0 = 0.5, \quad \boldsymbol{D}(\boldsymbol{u}) = 0.01.$$

17

	c_f				ϕ			
	no limiter		with limiter		no limiter		with limiter	
N	L^2 error	order	L^2 error	order	L^2 error	order	L^2 error	order
4	2.90e-1	–	9.48e-2	–	1.82e-1	–	1.11e-1	–
8	2.46e-2	3.56	1.21e-2	2.97	2.50e-2	2.87	1.50e-2	2.89
16	1.83e-3	3.74	1.16e-3	3.39	3.18e-3	2.97	1.91e-3	2.97
32	1.40e-4	3.71	1.47e-4	2.98	4.00e-4	2.99	2.39e-4	2.99
64	1.29e-5	3.47	1.53e-5	3.26	5.00e-5	3.00	2.99e-5	3.00
N	L^∞ error	order	L^∞ error	order	L^∞ error	order	L^∞ error	order
4	1.52e-1	–	2.45e-2	–	5.01e-2	–	2.64e-2	–
8	7.08e-3	4.42	3.61e-3	2.76	7.11e-3	2.82	3.98e-3	2.73
16	7.21e-4	3.29	6.21e-4	2.54	9.16e-4	2.96	5.20e-4	2.94
32	1.12e-4	2.69	1.33e-4	2.22	1.15e-4	2.99	6.56e-5	2.99
64	9.66e-6	3.53	1.53e-5	3.13	1.44e-5	3.00	8.22e-6	3.00

Table 1: Example 6.1: Accuracy test for c_f and ϕ with and without bound-preserving technique.

This example is used to demonstrate the necessity of the bound-preserving technique. The simulation will blow up without the technique due to the negativity of ϕ in some region while the bound-preserving scheme performs well.

We take $N = 40$ over the computational domain $\Omega = [0, 2\pi] \times [0, 2\pi]$. Moreover, we use P^1 element in this example since it is more suitable to demonstrate the stability than higher order ones, and set the time-step as small as $\Delta t = 0.001h^2$. All these effort is made to prevent the simulation without limiter from blowing up.

However, numerical simulation shows that the simulation without bound-preserving technique blows up at about $T = 0.0155$. The distributions of c_f before blow-up is shown in Figure 5. While with the

(a) c_f at $T = 0.005$s

(b) c_f at $T = 0.015$s
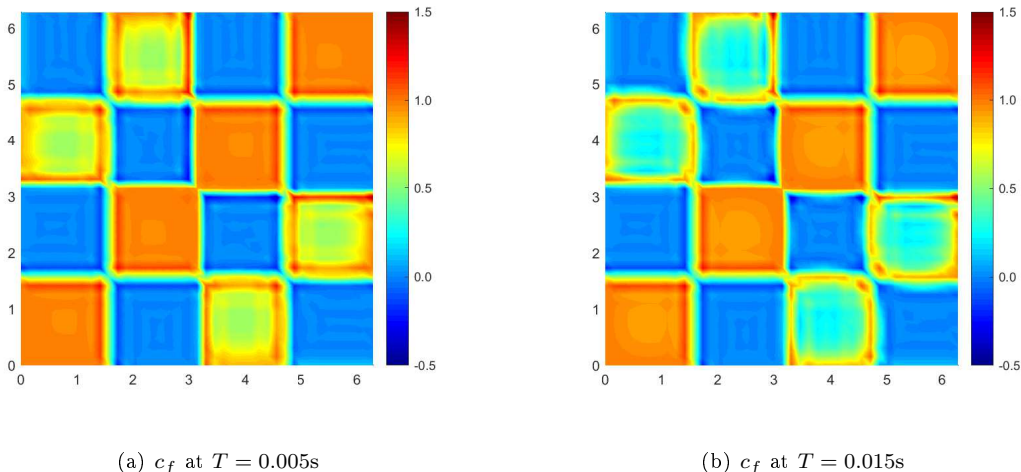
Figure 5: Evolution of c_f without limiter

settings exactly the same, the simulation with bound-preserving technique is stable. The distribution of c_f with time evolution in this case is given in Figure 6. We can see that the numerical approximations are high oscillatory. This is because the bound-preserving technique only preserves the bound but cannot suppress the oscillations. Some suitable limiters such as TVD, TVB and WENO limiters can suitably smooth the numerical approximations. Though oscillatory, the numerical simulation did not blow up. Therefore, with the bound-preserving technique, the numerical scheme is quite stable. What's more, we plot the evolution of extreme value of c_f and ϕ in Ω along simulation time in Figure 7 to illustrate the effectiveness of bound-preserving technique more clearly. We can observe that without the bound-preserving limiter, the concentration of acid c_f can be negative and greater than 1, and the porosity ϕ can also be negative, leading to ill-posed problems. With the bound-preserving technique, all the numerical approximations are within the physical bounds.

Example 6.3. *We simulate a single wormhole propagation experiment in rectangular rock tube, from which we can observe the formation and propagation of a wormhole starting from a singular point. The parameters*
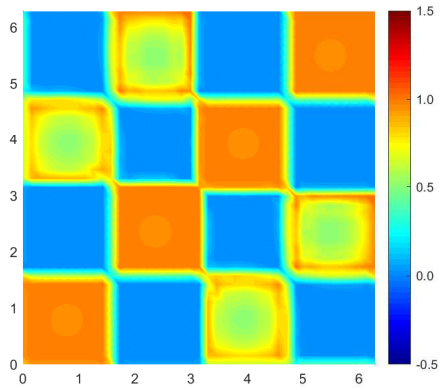
(a) c_f at $T = 0.005$s
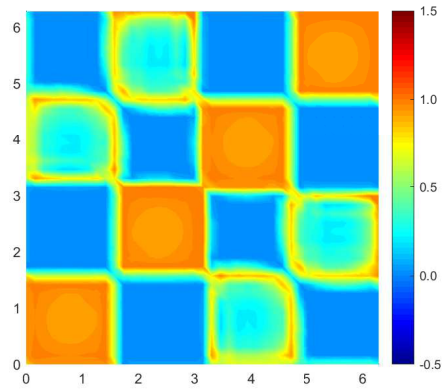
(b) c_f at $T = 0.015$s
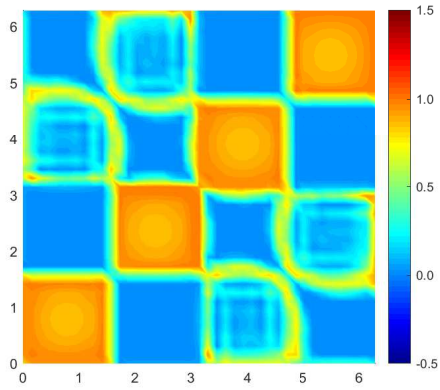
(c) c_f at $T = 0.030$s
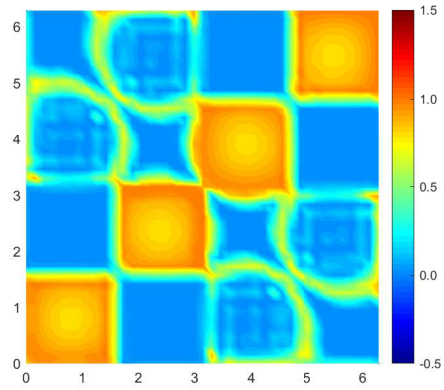
(d) c_f at $T = 0.050$s

Figure 6: Evolution of c_f with limiter.
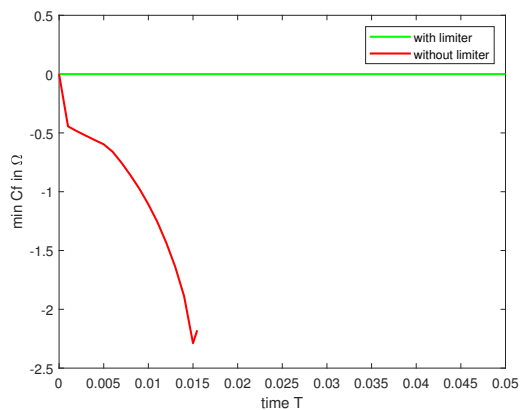
(a) Evolution of $\min\limits_{x\in\Omega} c_f(x,t)$
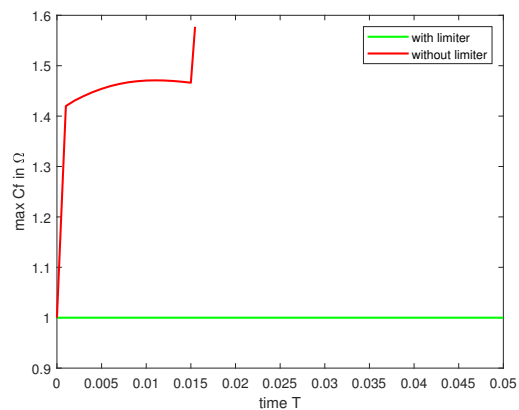
(b) Evolution of $\max\limits_{x\in\Omega} c_f(x,t)$
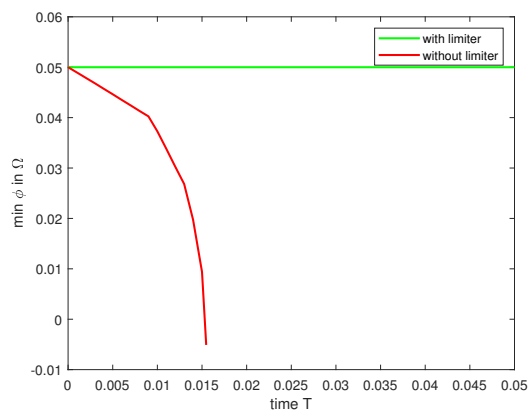
(c) Evolution of $\min\limits_{x\in\Omega} \phi(x,t)$
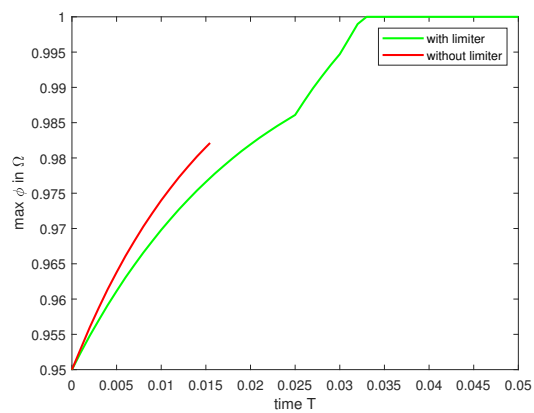
(d) Evolution of $\max\limits_{x\in\Omega} \phi(x,t)$

Figure 7: Evolution of extreme value of c_f and ϕ in Ω.

are taken as

$$\mathbf{D} = 0, \quad K_0 = 10^{-9}\mathrm{m}^2, \quad T = 15\mathrm{s},$$
$$\alpha = 100\mathrm{kg/mol}, \quad k_c = 1\mathrm{m/s}, \quad k_s = 10\mathrm{m/s},$$
$$\mu = 10^{-2}\mathrm{Pa\,s}, \quad f_I = f_p = 0, \quad c_{f0} = 0,$$
$$a_0 = 2\mathrm{m}^{-1}, \quad \rho_s = 2500\mathrm{kg/m}^2, \quad \phi_0 = 0.2,$$

Moreover, the computational domain is $\Omega = [0, 0.2\mathrm{m}] \times [0, 0.2\mathrm{m}]$. To investigate the phenomenon of wormhole propagation, we set a singular area with high porosity $\phi = 0.4$ and corresponding permeability determined by (2.5) which is about $10^{-8}\mathrm{m}^2$ on the middle of the left boundary with size $0.01\mathrm{m} \times 0.01\mathrm{m}$. The left and right boundary of the domain are Dirichlet conditions with pressure $p_d = 10000\mathrm{Pa}$ and $p_d = -10000\mathrm{Pa}$, respectively. The upper and lower boundaries of the domain are impermeable, i.e. $\boldsymbol{u} \cdot \boldsymbol{n} = 0$. The acid flows into the rock from the left boundary with a concentration of $c_I = 1\mathrm{mol/m}^2$ and drained out of it from the right boundary.

The contour plots of the concentration of acid and porosity of the rock at different time are shown in Figures 8-9, from which we can observe $c_f, \phi \in [0, 1]$ and the phenomenon of wormhole propagation along the whole simulation.

7   Concluding remarks

In this paper, we constructed high-order bound-preserving DG methods for wormhole propagation on triangular meshes. We have obtained the bound-preserving and monotone-increasing properties for concentration and porosity, respectively, with high-order accuracy. Numerical experiments have shown the accuracy and effectiveness of the bound-preserving technique.

References

[1] O.O. Akanni, H.A. Nasr-El-Din and D. Gusain, *A Computational Navier-Stokes Fluid-Dynamics-Simulation Study of Wormhole Propagation in Carbonate-Matrix Acidizing and Analysis of Factors Influencing the Dissolution Process*, SPE Journal, 22 (2017), 187962.

[2] Z. Chen, H. Huang and J. Yan, *Third order maximum-principle-satisfying direct discontinuous Galerkin methods for time dependent convection diffusion equations on unstructured triangular meshes*, Journal of Computational Physics, 308 (2016), 198-217.

[3] N. Chuenjarern, Z. Xu and Y. Yang *High-order bound-preserving discontinuous Galerkin methods for compressible miscible displacements in porous media on triangular meshes*, Journal of Computaitonal Physics, 378 (2019), 110-128.

[4] J. Du and Y. Yang, *Maximum-principle-preserving third-order local discontinuous Galerkin methods on overlapping meshes*, Journal of computational physics, 377 (2019), 117-141.
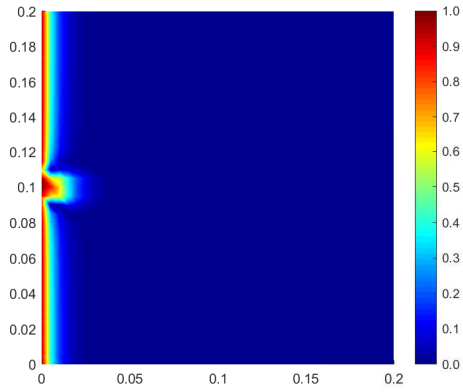
(a) c_f at $T = 1$s
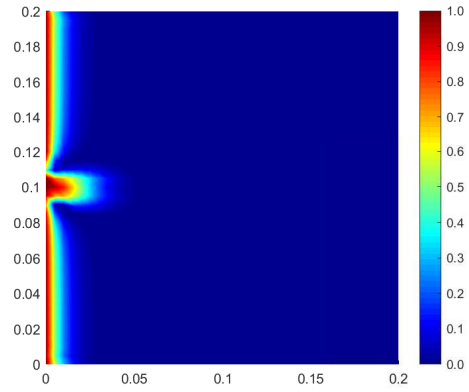
(b) c_f at $T = 5$s
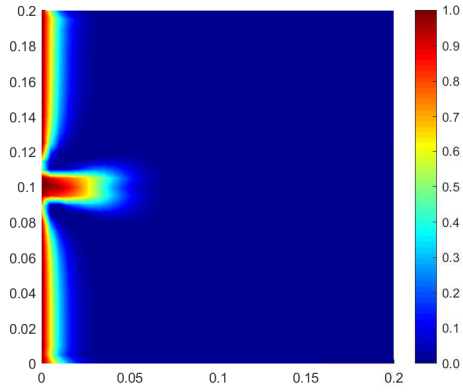
(c) c_f at $T = 10$s
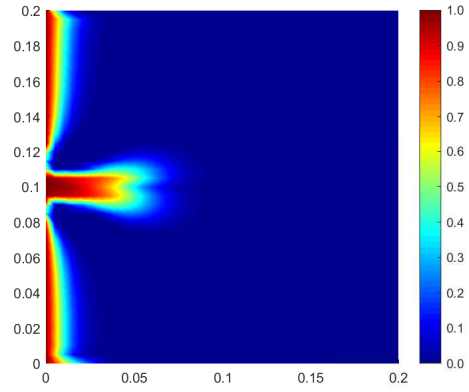
(d) c_f at $T = 15$s

Figure 8: Concentration of acid with time evolution.

(a) ϕ at $T = 1$s

(b) ϕ at $T = 5$s
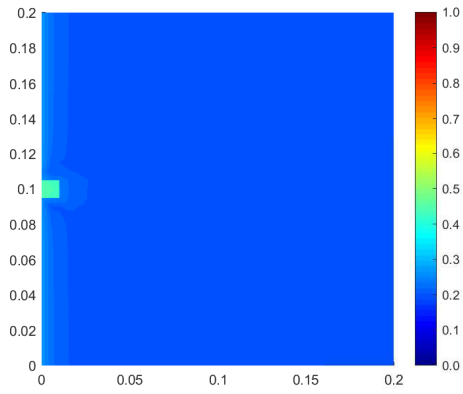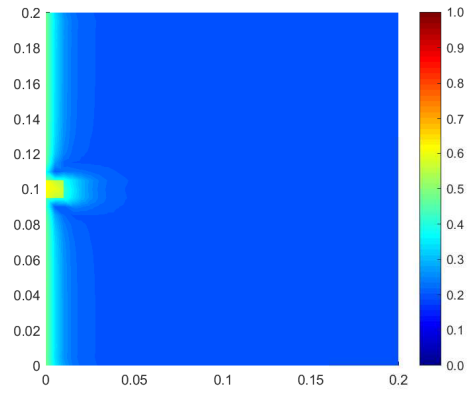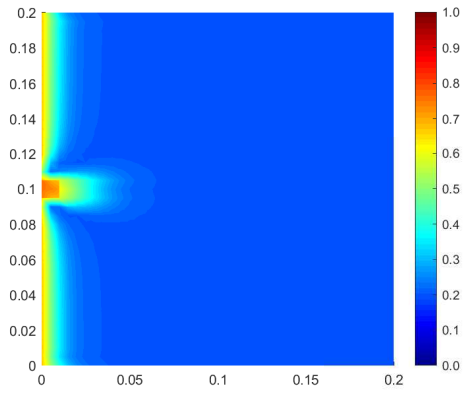
(c) ϕ at $T = 10$s
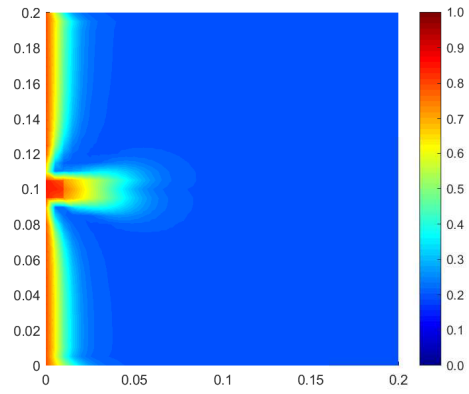
(d) ϕ at $T = 15$s

Figure 9: Porosity of rock with time evolution.

[5] C.N. Fredd and H.S. Fogler, *Influence of transport and reaction on wormhole formation in porous media*, AIChE journal, 44 (1998), 1933-1949.

[6] S. Gottlieb, D. Ketcheson and C.-W. Shu, *High order strong stability preserving time discretizations*, Journal of Scientific Computing, 38 (2009), 251-289.

[7] S. Gottlieb, C.-W. Shu and E. Tadmor, *Strong stability-preserving high-order time discretization methods*, SIAM review, 43 (2001), 89-112.

[8] H. Guo, L. Tian, Z. Xu, et. al., *High-order local discontinuous Galerkin method for simulating wormhole propagation*, Journal of Computational and Applied Mathematics, 350 (2019), 247-261.

[9] H. Guo and Y. Yang, *Bound-preserving discontinuous Galerkin method for compressible miscible displacement in porous media*, SIAM Journal on Scientific Computing, 39 (2017), A1969-A1990.

[10] L. Guo and Y. Yang, *Positivity preserving high-order local discontinuous Galerkin method for parabolic equations with blow-up solutions*, Journal of Computational Physics, 289 (2015), 181-195.

[11] M.L. Hoefner and H.S. Fogler, *Pore evolution and channel formation during flow and reaction in porous media*, AIChE Journal, 34 (1988), 45-54.

[12] J. Kou, S. Sun and Y. Wu, *Mixed finite element-based fully conservative methods for simulating wormhole propagation*, Computer Methods in Applied Mechanics and Engineering, 298 (2016), 279-302.

[13] X. Li and H. Rui, *Characteristic block-centered finite difference method for simulating incompressible wormhole propagation*, Computers and Mathematics with Applications, 73 (2017), 2171-2190.

[14] X. Li and H. Rui, *Block-Centered Finite Difference Method for Simulating Compressible Wormhole Propagation*, Journal of Scientific Computing, 74 (2018), 1115-1145.

[15] P. Maheshwari and V. Balakotaiah, *3D Simulation of carbonate acidization with HCl: comparison with experiments* In SPE Production and Operations Symposium. Society of Petroleum Engineers, 2013.

[16] M.K. Panga, M. Ziauddin and V. Balakotaiah, *Two-scale continuum model for simulation of wormholes in carbonate acidization* AIChE journal, 51 (2005), 3231-3248.

[17] T. Qin, C.-W. Shu and Y. Yang, *Bound-preserving discontinuous Galerkin methods for relativistic hydrodynamics*, Journal of Computational Physics, 315 (2016), 323–347.

[18] C.-W. Shu, *Total-variation-diminishing time discretizations*, SIAM Journal on Scientific and Statistical Computing, 9 (1988), 1073-1084.

[19] W. Wei, A. Varavei and K. Sepehrnoori, *Modeling and Analysis on the Effect of Two-Phase Flow on Wormhole Propagation in Carbonate Acidizing*, SPE Journal, 22 (2017), 186111.

[20] K. Wu, *Design of provably physical-constraint-preserving methods for general relativistic hydrodynamics*, Physical Review D, 95 (2017), 103001.

[21] Y. Wu, A. Salama and S. Sun, *Parallel simulation of wormhole propagation with the Darcy–Brinkman–Forchheimer framework*, Computers and Geotechnics, 69 (2015), 564-577.

[22] Y. Xing, X. Zhang and C.-W. Shu, *Positivity preserving high order well balanced discontinuous Galerkin methods for the shallow water equations*, Advances in Water Resources, 33 (2010), 1476–1493.

[23] T. Xiong, J.-M. Qiu and Z. Xu, *High order maximum-principle-preserving discontinuous Galerkin method for convection-diffusion equations*, SIAM Journal on Scientific Computing, 37 (2015), A583-A608.

[24] Z. Xu, *Parametrized maximum principle preserving flux limiters for high order schemes solving hyperbolic conservation laws: one-dimensional scalar problem*, Mathematics of Computation, 83 (2014), 310–331.

[25] S. Srinivasan, J. Poggie and X. Zhang, *A positivity-preserving high order discontinuous Galerkin scheme for convection-diffusion equations*, Journal of Computational Physics, 366 (2018), 120-143.

[26] Y. Yang and C.-W. Shu, *Discontinuous Galerkin method for hyperbolic equations involving δ-singularities: negative-order norm error estimates and applications*, Numerische Mathematik, 124 (2013), 753–781.

[27] Y. Yang, D. Wei and C.-W. Shu, *Discontinuous Galerkin method for Krause's consensus models and pressureless Euler equations*, Journal of Computational Physics, 252 (2013), 109–127.

[28] L. Zhang, T. Cui and H. Liu, *A set of symmetric quadrature rules on triangles and tetrahedra*, Journal of Computational Mathematics, 27 (2009), 89-96.

[29] X. Zhang and C.-W. Shu, *On maximum-principle-satisfying high order schemes for scalar conservation laws*, Journal of Computational Physics, 229 (2010), 3091-3120.

[30] X. Zhang, Y. Xia and C.-W. Shu, *Maximum-principle-satisfying and positivity-preserving high order discontinuous Galerkin schemes for conservation laws on triangular meshes*, Journal of Scientific Computing, 50 (2012), 29-62.

[31] X. Zhang and C.-W. Shu, *Positivity-preserving high order discontinuous Galerkin schemes for compressible Euler equations with source terms*, Journal of Computational Physics, 230 (2011), 1238-1248.

[32] Y. Zhang, X. Zhang and C.-W. Shu, *Maximum-principle-satisfying second order discontinuous Galerkin schemes for convection–diffusion equations on triangular meshes*, Journal of Computational Physics, 234 (2013), 295-316.

[33] C. Zhao, B.E. Hobbs, P. Hornby, et. al., *Theoretical and numerical analyses of chemical-dissolution front instability in fluid-saturated porous rocks*, International Journal for Numerical and Analytical Methods in Geomechanics, 32 (2008), 1107-1130.

[34] X. Zhao, Y. Yang and C. Seyler, *A positivity-preserving semi-implicit discontinuous Galerkin scheme for solving extended magnetohydrodynamics equations*, Journal of Computational Physics, 278 (2014), 400-415.